Article

Synthesis of Atomically Ordered AuCu and AuCu Nanocrystals from Bimetallic Nanoparticle Precursors

Amandeep K. Sra, and Raymond E. Schaak

J. Am. Chem. Soc., **2004**, 126 (21), 6667-6672• DOI: 10.1021/ja031547r • Publication Date (Web): 07 May 2004

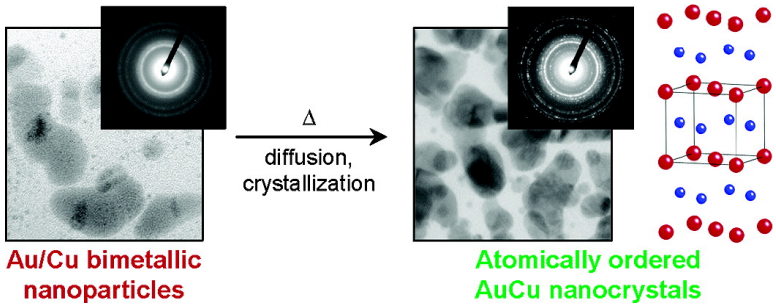

More About This Article

Additional resources and features associated with this article are available within the HTML version:

- Supporting Information
- Links to the 7 articles that cite this article, as of the time of this article download
- Access to high resolution figures
- Links to articles and content related to this article
- Copyright permission to reproduce figures and/or text from this article

View the Full Text HTML

J|A|C|S
ARTICLES
Published on Web 05/07/2004

Synthesis of Atomically Ordered AuCu and $AuCu_3$ Nanocrystals from Bimetallic Nanoparticle Precursors

Amandeep K. Sra and Raymond E. Schaak*

Contribution from the Department of Chemistry, Texas A&M University, College Station, Texas 77842-3012

Received December 5, 2003; E-mail: schaak@mail.chem.tamu.edu

Abstract: A new multistep approach was developed to synthesize atomically ordered intermetallic nanocrystals, using AuCu and $AuCu_3$ as model systems. Bimetallic nanoparticle aggregates are used as precursors to atomically ordered nanocrystals, both to precisely define the stoichiometry of the final product and to ensure that atomic-scale diffusion distances lower the reaction temperatures to prevent sintering. In a typical synthesis, PVP-stabilized Au−Cu nanoparticle aggregates synthesized by borohydride reduction are collected by centrifugation and annealed in powder form. At temperatures below 175 °C, diffusion of Cu into Au occurs, and the atomically disordered solid solution Cu_xAu_{1-x} exists. For AuCu, nucleation occurs by 200 °C, and atomically ordered AuCu exists between 200 and 400 °C. For $AuCu_3$, an AuCu intermediate nucleates at 200 °C, and further diffusion of Cu into the AuCu intermediate at 300 °C nucleates $AuCu_3$. Atomically ordered AuCu and $AuCu_3$ nanocrystals can be redispersed as discrete colloids in solution after annealing between 200 and 300 °C.

Introduction

The recent interest in using nanocrystalline inorganic solids as building blocks for new nanoscale devices and technologies has spawned an enormous research effort aimed at developing selective syntheses of inorganic nanocrystals.[1] In this regard, significant progress has been made in controlling the chemistry of nanoscale solid-state materials[2] and in understanding their unique size-dependent properties.[3−5] The primary goal of much of the current research in this area involves controlling the *external* structure of nanocrystals (e.g., shape, size, and uniformity), which is necessary for exploiting anisotropic structure−property relationships and for using nanocrystals in future technological applications.[6] However, controlling the *internal* structure of nanocrystals, which directly influences their physical properties, is an equally important aspect of nanocrystal synthesis. In bulk solids, the crystallographic ordering of atoms is the most critical factor in determining the properties of a material, since the directional overlap of atomic orbitals determines its band structure and thus its properties. In the nanoscopic size regime, where size and shape can influence the properties of a material through quantum effects,[3] controlling the crystallographic ordering of atoms has received much less attention.

Among the most important for the myriad applications of nanomaterials are the atomically ordered intermetallic compounds of the late transition metals, which remain impossible to synthesize as solution-dispersible nanocrystals. While most reports of bimetallic nanocrystals involve atomically *disordered* alloys,[7] a few have succeeded at transforming disordered alloys into ordered intermetallic compounds.[8−10] For example, Sun and co-workers accessed the ordered face-centered tetragonal (fct) form of FePt by annealing a spin-cast film of atomically disordered FePt nanocrystals at high temperatures.[8,9] As synthesized, the atomically disordered FePt nanocrystals are superparamagnetic, but transform to ferromagnetic FePt nanocrystals with high coercivity and high magnetic anisotropy after annealing above 550 °C.[8] Likewise, Teng and Yang recently transformed Pt−Fe_2O_3 core−shell nanoparticles into atomically

(1) Murray, C. B.; Kagan, C. R.; Bawendi, M. G. *Annu. Rev. Mater. Sci.* **2000**, *30*, 545−610.
(2) (a) Murray, C. B.; Sun, S.; Gaschler, W.; Doyle, H.; Betley, T. A.; Kagan, C. R. *IBM J. Res. Dev.* **2001**, *45*, 47−55. (b) Trindade, T.; O'Brien, P.; Pickett, N. L. *Chem. Mater.* **2001**, *13*, 3843−3858. (c) Rogach, A. L.; Talapin, D. V.; Shevchenko, E. V.; Kornowski, A.; Haase, M.; Weller, H. *Adv. Funct. Mater.* **2002**, *12*, 653−664. (d) Hyeon, T. *Chem. Commun.* **2003**, 927−934.
(3) (a) Alivisatos, A. P. *Science* **1996**, *271*, 933−937. (b) Efros, Al. L.; Rosen, M. *Annu. Rev. Mater. Sci.* **2000**, *30*, 475−521. (c) Hu, J.; Wang, L.-W.; Li, L.-S.; Yang, W.; Alivisatos, A. P. *J. Phys. Chem. B* **2002**, *106*, 2447−2452.
(4) (a) Vestal, C. R.; Zhang, Z. J. *Chem. Mater.* **2001**, *13*, 2092−2096. (b) Vestal, C. R.; Zhang, Z. J. *Chem. Mater.* **2002**, *14*, 3817−3822.
(5) Roucoux, A.; Schulz, J.; Patin, H. *Chem. Rev.* **2002**, *102*, 3757−3778.
(6) (a) Manna, L.; Scher, E. C.; Alivisatos, A. P. *J. Am. Chem. Soc.* **2000**, *122*, 12700−12706. (b) Puntes, V. F.; Krishnan, K. M.; Alivisatos, A. P. *Science* **2001**, *291*, 2115−2118. (c) Jana, N. R.; Gearheart, L.; Obare, S. O.; Murphy, C. J. *Langmuir* **2002**, *18*, 922−927. (d) Sun, Y.; Xia, Y. *Science* **2002**, *298*, 2176−2180. (e) Scher, E. C.; Manna, L.; Alivisatos, A. P. *Philos. Trans. R. Soc. London, Ser. A* **2003**, *361*, 241−257.
(7) (a) Sangregorio, C.; Galeotti, M.; Bardi, U.; Baglioni, P. *Langmuir* **1996**, *12*, 5800−5802. (b) Link, S.; Wang, Z. L.; El-Sayed, M. A. *J. Phys. Chem. B* **1999**, *103*, 3529−3533. (c) Shevchenko, E. V.; Talapin, D. V.; Rogach, A. L.; Kornowski, A.; Haase, M.; Weller, H. *J. Am. Chem. Soc.* **2002**, *124*, 11480−11485. (d) Fang, J.; Tung, L. D.; Stokes, K. L.; He, J.; Caruntu, D.; Zhou, W. L.; O'Connor, C. J. *J. Appl. Phys.* **2002**, *91*, 8816−8818. (e) Shevchenko, E. V.; Talapin, D. V.; Schnablegger, H.; Kornowski, A.; Festin, O.; Svedlindh, P.; Haase, M.; Weller, H. *J. Am. Chem. Soc.* **2003**, *125*, 9090−9101. (f) Hambrock, J.; Schroter, M. K.; Birkner, A.; Woll, C.; Fischer, R. A. *Chem. Mater.* **2003**, *15*, 4217−4222. (g) Kim, M.-J.; Na, H.-J.; Lee, K. C.; Yoo, E. A.; Lee, M. *J. Mater. Chem.* **2003**, *13*, 1789−1792. (h) Zitoun, D.; Amiens, C.; Chaudret, B.; Fromen, M.-C.; Lecante, P.; Casanove, M.-J.; Respaud, M. *J. Phys. Chem. B* **2003**, *107*, 6997−7005. (i) Mandal, M.; Kundu, S.; Sau, T. K.; Yusuf, S. M.; Pal, T. *Chem. Mater.* **2003**, *15*, 3710−3715.
(8) Sun, S.; Murray, C. B.; Weller, D.; Folks, A.; Moser, A. *Science* **2000**, *287*, 1989−1992.
(9) Elkins, K. E.; Vedantam, T. S.; Liu, J. P.; Zeng, H.; Sun, S.; Ding, Y.; Wang, Z. L. *Nano Lett.* **2003**, *3*, 1647−1649.
(10) Teng, X.; Yang, H. *J. Am. Chem. Soc.* **2003**, *125*, 14559−14563.

ordered fct FePt nanocrystals by high-temperature (550 °C) reduction and annealing of a surface-confined monolayer film.[10]

These methods prove the feasibility of solid-state transformations in nanocrystals and attest to the enhanced properties that can be achieved through such reactions. However, there remain several critical limitations. The high annealing temperatures remove the stabilizing ligands (or thermally decompose the organic ligands into a carbide coating[8]), preventing redispersion in solution for high-volume applications. The high annealing temperatures also tend to significantly increase the crystallite size through sintering. As a result, only surface-confined nanocrystals have been amenable to solid-state transformations,[8−11] since multilayer films and bulk powders significantly coalesce at high temperatures.

To prevent the detrimental effects of sintering on the morphology of internally structured nanocrystals and nanocrystalline films, new lower-temperature routes to atomically ordered nanocrystals are necessary. To that end, we report here a new multistep approach to the synthesis of intermetallic nanocrystals that relies on the low-temperature annealing of bimetallic nanoparticle precursors. Since FePt and other interesting magnetic alloys crystallize in the AuCu and related $AuCu_3$ structure types,[12] we focused on Au−Cu as a model binary system. By utilizing two-component nanoparticle aggregates as synthetic precursors, we can control the stoichiometry and diffusion distances to yield atomically ordered nanocrystals of AuCu and $AuCu_3$ at temperatures of 200−300 °C. Many other binary transition metal systems have similar atomically ordered structures in the same temperature range,[12,13] so we believe this approach could be extended to the synthesis of a wide range of intermetallic nanocrystals (although differences in activation barriers would reasonably require different annealing temperatures depending on the particular binary system). Furthermore, since AuCu and $AuCu_3$ are normally prepared by annealing premelted Au−Cu samples (melted > 850 °C) for several days or weeks, we believe that this approach may also be applicable as a new low-temperature route to intermetallic compounds that are not thermodynamically stable.

Experimental Section

Nanoparticles of AuCu were synthesized using a modification of the approach described by Lu et al. for the synthesis of Pd nanocrystals.[14] Copper acetate [$Cu(C_2H_3O_2)_2$, 6.8 mg] and poly(vinylpyrrolidone) (PVP, 460 mg) were added to 25 mL of distilled, deionized water (NANOpure, 18.2 MΩ). After the mixture was stirred under Ar for 20−30 min, 25 mL of 0.01 M $NaBH_4$ was added. The color quickly changed from faint blue to yellow-orange, indicating reduction of Cu^{2+} to Cu^0. After 20 min of stirring under Ar, $HAuCl_4 \cdot 3H_2O$ (13.3 mg) in 5 mL of water was injected, and the solution turned dark red, indicating reduction of Au^{3+} to Au^0. (The order of metal salt addition does not rigorously matter. Gold can be reduced first, or gold and copper can both be reduced at the same time, and the results are similar.) Over 2 h, the color of the Cu−Au solution gradually changed from dark red to dark brown/black, suggesting a reaction between the Au and Cu nanoparticles, most likely at their surfaces to form aggregate structures. (This solution is stable for several days, in contrast to the solution formed from only the reduction of copper acetate, which turned yellow over the same time period due to the formation of Cu_2O.) AuCu powder was isolated by centrifuging the Au−Cu solution, and then washing several times with water and ethanol. $AuCu_3$ nanoparticles were prepared in the same way, using 10.1 mg of $Cu(C_2H_3O_2)_2$ and 6.7 mg of $HAuCl_4 \cdot 3H_2O$ to yield a 3:1 Cu:Au ratio.

Dried powders of AuCu and $AuCu_3$ were heated in a tube furnace under flowing argon in the temperature range 50−500 °C for 2−12 h. (The presence of Cu_2O was always detected in annealed samples of $AuCu_3$, suggesting that some Cu remains exposed on the surface of the Au−Cu_3 nanoparticle aggregates. In contrast, Cu_2O was not detected in any annealed samples of AuCu, suggesting that Au completely passivates the surface of the nanoparticle aggregates.) The AuCu samples heated to 200 °C and $AuCu_3$ samples heated to 300 °C were resuspended in ethanol by sonicating 5 mg of annealed powder in 2 mL of ethanol.

Powder X-ray diffraction (XRD) data were collected on a Bruker GADDS three-circle X-ray diffractometer using Cu Kα radiation. High-resolution transmission electron microscopy (TEM) images, energy-dispersive X-ray spectroscopy (EDS) analysis, and electron diffraction data were collected on a JEOL JEM-2010 TEM. Samples for EDS analysis were deposited on Ni TEM grids to avoid erroneously detecting Cu from the traditional Cu grids. UV−visible spectroscopic data were obtained on a Jasco V-530 UV−visible spectrophotometer. Elemental analysis (CHN) was performed by Atlantic Microlab (Norcross, GA).

Results and Discussion

Synthesis of AuCu and $AuCu_3$ Nanocrystals. Figure 1 shows our approach to the synthesis of atomically ordered AuCu and $AuCu_3$ nanocrystals using bimetallic precursors. First, PVP-stabilized Cu nanoparticles are formed by the aqueous borohydride reduction of copper acetate, and the solution turns yellow-orange, consistent with reduction from Cu^{2+} to Cu^0. After adding a stoichiometrically controlled amount of $HAuCl_4 \cdot 3H_2O$, Au nanoparticles form via borohydride reduction, and the solution changes to a deep orange-red color, suggesting the presence of a mixture of Au and Cu nanoparticles. Over the next 2 h, the color of the solution gradually changes from orange-red to brown-black, and the solution is stable for at least 1 day before significant aggregation and precipitation occur. (PVP-stabilized Cu nanoparticles synthesized without the addition of Au quickly oxidize to Cu_2O, as evidenced by XRD analysis and a change in color.) After aging for several hours, the Au−Cu composite particles are collected by centrifugation and isolated as a powder. Following annealing under an inert atmosphere, nucleation of atomically ordered AuCu or $AuCu_3$ occurs (depending on the starting stoichiometry), and the nanocrystals can subsequently be resuspended in solution by sonication.

Visible absorption spectra for our samples are shown in Figure 2. A solution of Au nanoparticles (without Cu) shows a broad maximum near 530 nm, with overall high absorbance in the 400−600 nm range. Cu (without Au) shows high absorbance between 400 and 500 nm. The 1:1 and 1:3 mixtures of Au:Cu have features resembling those of both Au and Cu, along with broader absorbance maxima in the 550−650 nm range. For AuCu, the absorbance changes slightly over 3 h to show higher absorbance between 500 and 800 nm, which correlates with the observed change from an initial color of dark red to dark brown-black after aging. A similar shift in the absorbance profile is observed for the $AuCu_3$ sample.

(11) (a) Chen, M.; Nikles, D. E. *Nano Lett.* **2002**, *2*, 211−214. (b) Chen, M.; Nikles, D. E. *J. Appl. Phys.* **2002**, *91*, 8477−8479.
(12) Villars, P., Calvert, L. D., Eds. *Pearson's Handbook of Crystallographic Data for Intermetallic Phases*, 2nd ed.; ASM International: Materials Park, OH, 1991.
(13) Massalski, T. B., Ed. *Binary Alloy Phase Diagrams*; ASM International: Materials Park, OH, 1996.
(14) Lu, W.; Wang, B.; Wang, K.; Wang, X.; Hou, J. G. *Langmuir* **2003**, *19*, 5887−5891.

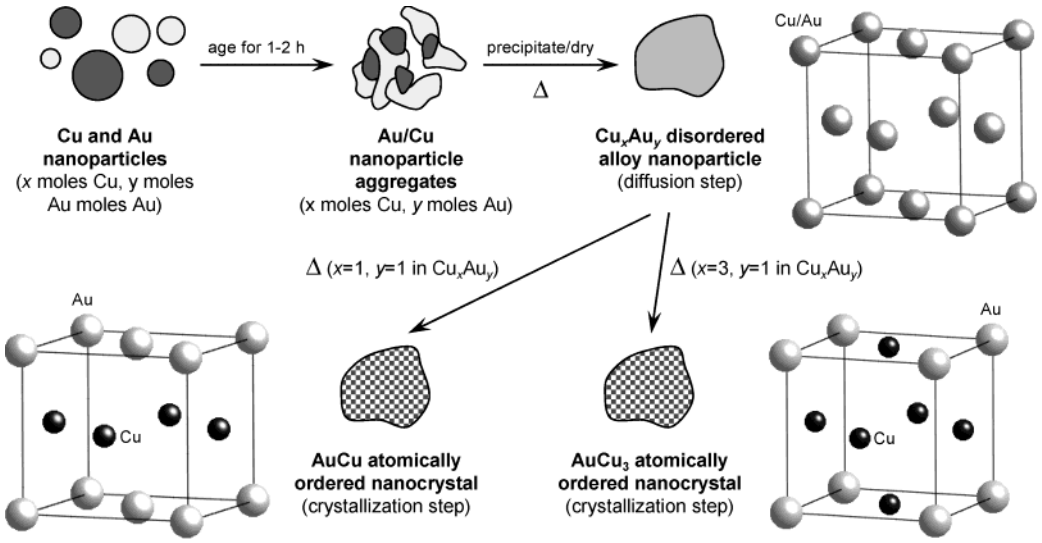

Figure 1. Idealized schematic of the multistep approach to the synthesis of atomically ordered nanocrystals from bimetallic nanoparticle aggregates. The crystal structures of Cu_xAu_y (fcc), AuCu (tetragonal), and $AuCu_3$ (cubic) are shown for comparison.

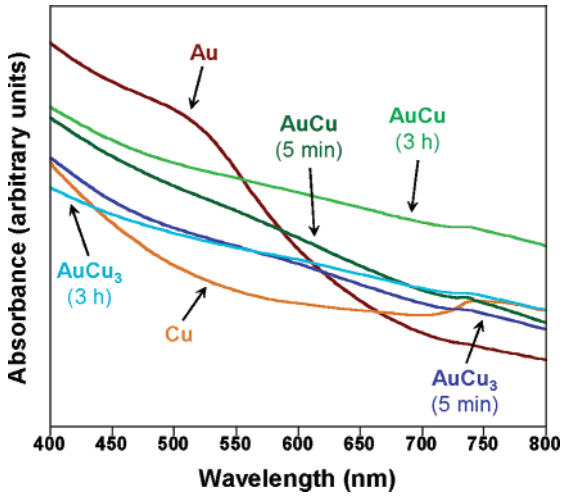

Figure 2. Visible absorption spectra for dilute nanoparticle solutions of Au and Cu nanoparticles, along with 1:1 and 1:3 mixtures of Au and Cu nanoparticles after 5 min and 3 h. The absorption feature near 735 nm is an instrumental artifact.

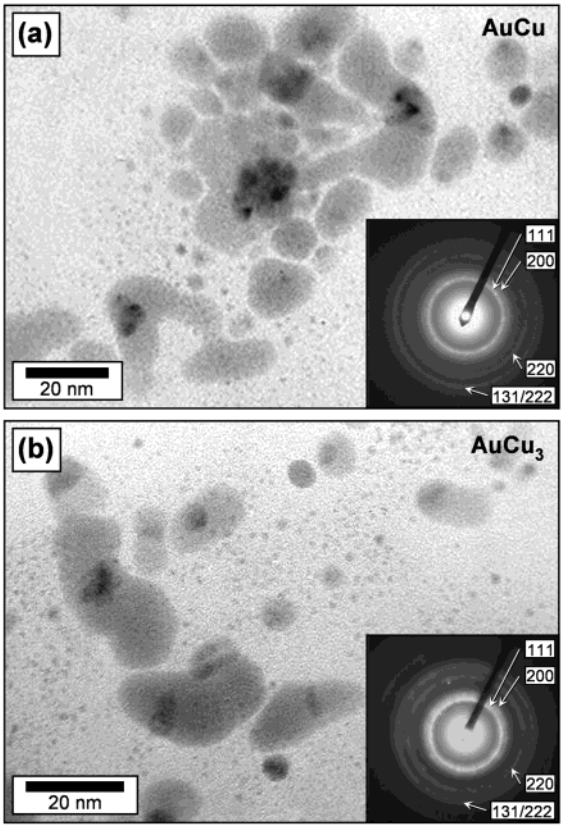

Figure 3. TEM micrographs of (a) AuCu and (b) $AuCu_3$ nanoparticle aggregates synthesized by allowing a solution of PVP-stabilized Au and Cu nanoparticles synthesized by borohydride reduction to age for 2 h. Selected area electron diffraction patterns are shown in the insets.

TEM micrographs of the AuCu and $AuCu_3$ nanoparticle aggregates at room temperature (Figures 3 and 4) clearly show a contrast difference within the individual particles. This suggests that the Cu and Au remain segregated, but are connected together through their surfaces as irregularly shaped aggregates. Qualitative EDS spectra recorded for individual AuCu and $AuCu_3$ nanoparticles show that both Au and Cu are present. Since Au has a higher electron density than Cu, the darker regions in the TEM micrographs may be expected to correspond to Au, which is verified by combining data from EDS, XRD, and electron diffraction analyses (discussed below). The reason for the nanoparticle aggregation is not yet clear, but it may be due to the higher interfacial free energy of Cu relative to Au.

The TEM micrographs in Figure 3 show AuCu and $AuCu_3$ nanoparticle aggregates as prepared in solution (prior to collection by centrifugation). Large binary nanoparticle aggregates can be seen, along with smaller spherical particles, most likely corresponding to Au and Cu nanoparticles (based on comparisons with control experiments involving the synthesis of pure Au and Cu nanoparticles). This indicates, as expected, that borohydride reduction forms a mixture of Au and Cu nanoparticles in addition to the bimetallic nanoparticle aggregates that form upon aging. Centrifugation collects the larger nanoparticle aggregates as a precipitate, leaving the smaller Au and Cu nanoparticles in solution. (The supernatant remains colored after centrifugation.) This indicates that the precipitate, which is used for the subsequent thermal transformation reaction, consists almost entirely of the larger nanoparticle aggregates, while the smaller unreacted Au and Cu nanoparticles remain in solution.

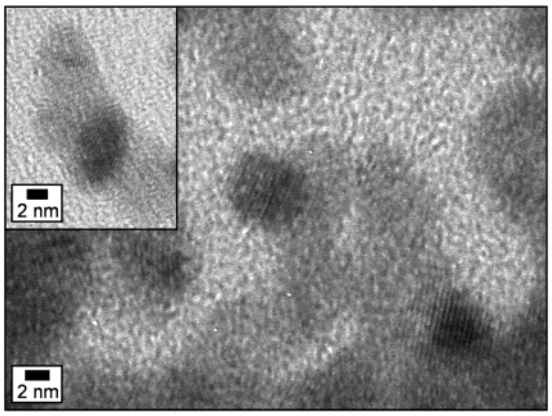

Figure 4. High-resolution TEM micrographs of AuCu nanoparticle aggregates, showing lattice fringes for only the Au nanocrystallites.

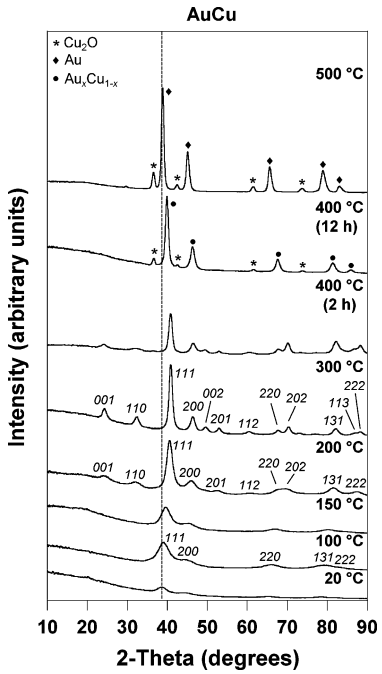

Figure 5. Powder XRD patterns for AuCu nanoparticles at 20 °C and annealed under Ar to temperatures between 100 and 500 °C.

The electron diffraction patterns in Figure 3 confirm a single-phase face-centered cubic structure for both the AuCu and the $AuCu_3$ nanoparticle aggregates. While both Au and Cu are present in reduced form, only Au is crystalline, which is confirmed by both the single-phase electron diffraction pattern in Figure 3 and the room-temperature XRD data in Figure 5. The high-resolution TEM micrographs in Figure 4 show lattice fringes for portions of the bimetallic nanoparticle aggregates, and these lattice fringes are equally spaced in all of the crystalline regions. Since the XRD data in Figure 5 clearly show the presence of Au and not Cu, the Cu is amorphous and the crystalline regions (which appear darker in the TEM micrographs) most likely correspond to Au.

Structural Characterization. The XRD patterns for samples of PVP-stabilized AuCu nanoparticles that were collected by centrifugation and annealed under Ar at a variety of temperatures are shown in Figure 5. At room temperature, XRD analysis yields a face-centered cubic (fcc) pattern ($a = 4.04$ Å) that is single-phase and nearly identical to that of Au (fcc, $a_{lit} = 4.078$ Å),[12] indicating that the Cu is amorphous and that some Cu is dissolved in the Au. Annealing at 100 and 150 °C retains the simple single-phase fcc pattern, but decreases the lattice constant to $a = 4.00$ Å and $a = 3.94$ Å, respectively. The decrease in the lattice constant with increasing temperature suggests that Cu is diffusing into the Au, forming the disordered solid solution Cu_xAu_{1-x}. By 200 °C, atomically ordered AuCu is present ($a = 3.96$ Å, $c = 3.64$ Å), and every peak in the XRD pattern indexes to the pattern expected for tetragonal AuCu ($a_{lit} = 3.963$ Å, $c_{lit} = 3.671$ Å).[12]

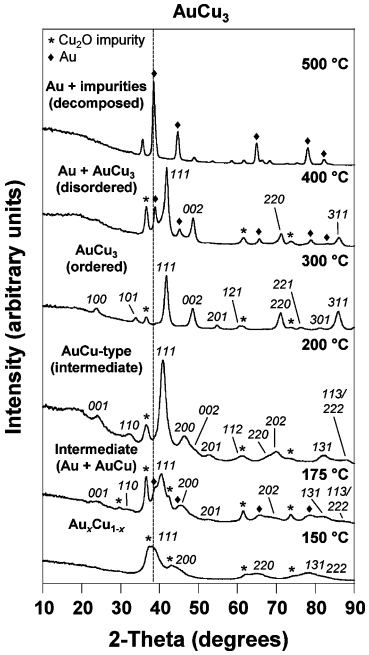

Figure 6. Powder XRD patterns for $AuCu_3$ nanoparticles annealed under Ar to temperatures between 150 and 500 °C.

As evident from the XRD data in Figure 5, heating to 300 °C retains the ordered AuCu structure, although the peaks begin to narrow, indicating an increase in the crystallite size. Persistence of nanocrystallinity during low-temperature annealing most likely results from crystallite confinement induced by the polymer (PVP) network. Short heating at 400 °C still shows the presence of atomically ordered AuCu. However, the superlattice reflections (*001* and *110*) are broadened, which suggests that the ordered structure is starting to either disorder or decompose. Longer heating times reveal the disappearance of all of the reflections related to the tetragonal structure of AuCu, leaving behind a simple fcc pattern with $a = 3.91$ Å. This is consistent with a disordered Au_xCu_{1-x} solid solution. By 500 °C, the fcc pattern yields $a = 4.01$ Å, indicating nearly complete decomposition to Au. The presence of Cu_2O rather than Cu upon decomposition is due to oxidation in air during sample handling or from microscopic oxygen contamination in the tube furnace.

When the molar ratio of Cu:Au is 3:1, annealing produces atomically ordered nanocrystals with the $AuCu_3$ structure. Figure 6 shows the temperature-dependent XRD patterns for $AuCu_3$ samples heated under Ar. As for AuCu, low-temperature annealing of $AuCu_3$ yields a single-phase fcc solid solution with $a = 4.04$ Å (at 150 °C), which is intermediate between the lattice constants of Au and Cu ($a_{lit} = 3.615$ Å).[12] A Cu_2O impurity is present in all samples of $AuCu_3$.

The XRD data for $AuCu_3$ samples annealed at temperatures between 175 and 300 °C provide insight into the mechanism

of the thermal transformation that converts a bimetallic nanoparticle aggregate into an atomically ordered nanocrystal. Heating $AuCu_3$ to 175 °C produces a mixture of phases − Au metal, AuCu, and Cu (as Cu_2O from oxidation). Further heating at 200 °C transforms $AuCu_3$ into a well-ordered AuCu-type intermediate. Since AuCu is tetragonal ($a_{lit} = 3.963$ Å, $c_{lit} = 3.671$ Å) and $AuCu_3$ is cubic ($a_{lit} = 3.749$ Å),[12] the presence of the AuCu intermediate ($a = 3.99$, $c = 3.64$) is clearly established by the XRD data and is most easily observed by the splitting of the *200*/*002* and *220*/*202* reflections, as well as the shift of the *111* reflection relative to that expected for $AuCu_3$. By 300 °C, the tetragonal AuCu-type intermediate converts to the cubic $AuCu_3$ phase ($a = 3.75$ Å).

At 150 °C, the Cu has clearly diffused into the Au, since the lattice constant is smaller than that of pure Au. At 175 °C, AuCu begins to crystallize, even though the overall stoichiometry of Cu:Au is 3:1. The diffusion of Cu into Au appears to set up a concentration gradient, and AuCu begins to nucleate when the interface reaches the appropriate 1:1 stoichiometry. The Au and Cu that are outside of the interfacial region remain as nearly-pure metals. By 200 °C, enough Cu has diffused into the Au to tie up all of the Au in the AuCu intermediate, so Au metal is no longer present in the XRD data. By 300 °C, all of the Cu has diffused into the AuCu intermediate, establishing the desired composition and nucleating cubic $AuCu_3$.

Interestingly, heating to 400 °C produces a simple fcc phase with $a = 3.74$ Å, which is nearly identical to the lattice constant for ordered $AuCu_3$. The absence of superlattice peaks suggests that the atomically disordered $AuCu_3$ phase exists at 400 °C, while the atomically ordered $AuCu_3$ phase exists below this temperature. This is consistent with the equilibrium phase diagram for the binary Au−Cu system,[13] which exhibits a well-known order/disorder phase transition just below 400 °C. The order/disorder phase transition appears to be present in $AuCu_3$ nanocrystals, although the size-dependence of this transition remains to be established. Above 500 °C, complete decomposition to Au and Cu (in the oxidized form, as Cu_2O) occurs.

Redispersion in Solution. The atomically ordered AuCu and $AuCu_3$ nanocrystals can be redispersed as discrete colloids in solution after annealing, which is impossible using higher-temperature annealing methods that irreversibly sinter bulk powders and multilayer films of nanocrystals. (Elemental analysis for CHN confirms that the PVP is not removed during annealing at or below 300 °C.) The TEM micrograph and corresponding electron diffraction pattern of AuCu nanoparticle aggregates in Figure 3a show that the nanocrystals are generally in the range of 15−30 nm and that they possess a disordered fcc structure. After annealing at 275 °C, the atomically ordered AuCu nanocrystals were redispersed in solution by sonication, and the nanocrystals appear to have retained their general shape and size distribution that was present before annealing. The TEM micrograph in Figure 7a shows the resuspended AuCu nanocrystals, which have a slightly larger average size of 20−25 nm. The contrast differences within and among the nanoparticles are a common feature of TEM analysis and can be caused by twinning, diffraction effects, and crystallite orientation, among other factors.[15] Similar contrast differences are seen in other nanocrystalline systems prepared using related annealing methods.[7d,10,16] The lattice fringes observed during high-resolution TEM analysis (Figure 7b) confirm that the AuCu

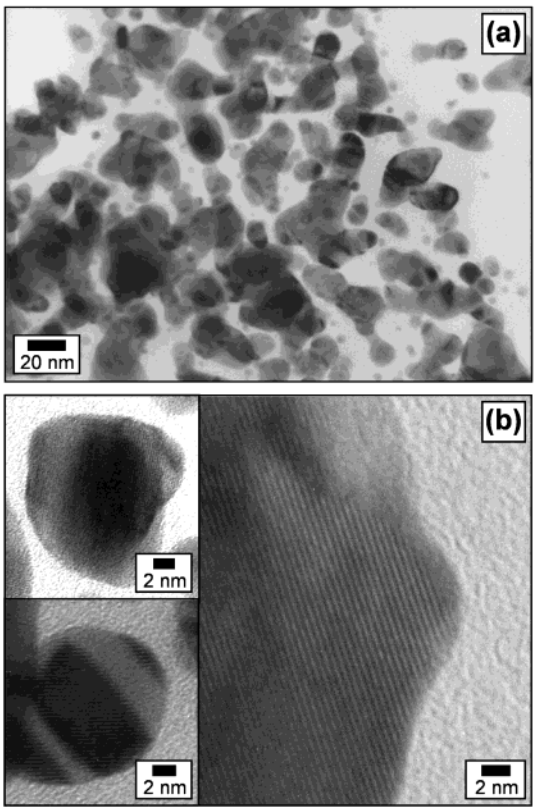

Figure 7. TEM micrographs of atomically ordered AuCu nanocrystals. A collection of nanocrystals is shown in (a), and high-resolution images of individual nanocrystals are shown in (b). The lattice fringes in (b) highlight the uniform crystallinity of the nanocrystals.

nanocrystals are highly crystalline. Furthermore, the fact that the lattice fringes uniformly penetrate the light and dark regions of the nanocrystals in a continuous manner attests to the formation of an alloyed phase and suggests that the contrast differences originate from the artifacts of TEM analysis described above (e.g., twinning, evident in the bottom inset of Figure 7b). This is in contrast to the light and dark regions of the nanoparticle aggregate precursors shown in Figure 3, which have lattice fringes that penetrate only the dark regions.

The corresponding electron diffraction pattern (Figure 8) is consistent with the XRD data in Figure 5, indicating an atomically ordered fct crystal structure. The electron diffraction pattern in Figure 8, prepared for TEM analysis by drying the redispersed AuCu nanocrystal solution on a TEM grid, unambiguously confirms that the nanocrystals annealed at 275 °C and resuspended in solution are atomically ordered. In particular, the superlattice reflections (*001* and *110*) and split reflections due to tetragonal symmetry (*200*/*002* and *220*/*202*) are highly visible. The TEM micrograph and electron diffraction pattern in Figure 9, showing the cubic superstructure of the ordered $AuCu_3$ phase, confirm that the $AuCu_3$ nanocrystals (annealed at 300 °C) can also be redispersed in solution. This clearly indicates that the atomically ordered nanocrystals can be redispersed in solution after bulk solid-state annealing, which means that the nanocrystals can be used in high-volume applications.

(15) Fultz, B.; Howe, J. M. *Transmission Electron Microscopy and Diffractometry of Materials*, 1st ed.; Springer-Verlag: Berlin, 2001.
(16) Black, C. T.; Murray, C. B.; Sandstrom, R. L.; Sun, S. *Science* **2000**, *290*, 1131−1134.

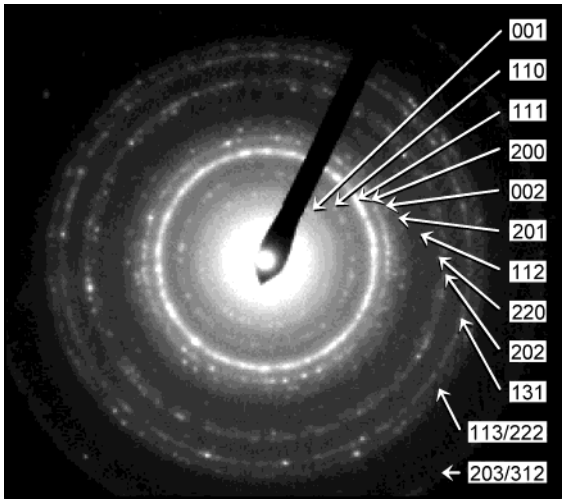

Figure 8. Electron diffraction pattern of AuCu nanocrystals that were annealed at 275 °C and redispersed in ethanol. The tetragonal symmetry and superlattice reflections of the atomically ordered AuCu structure are clearly evident in the diffraction pattern.

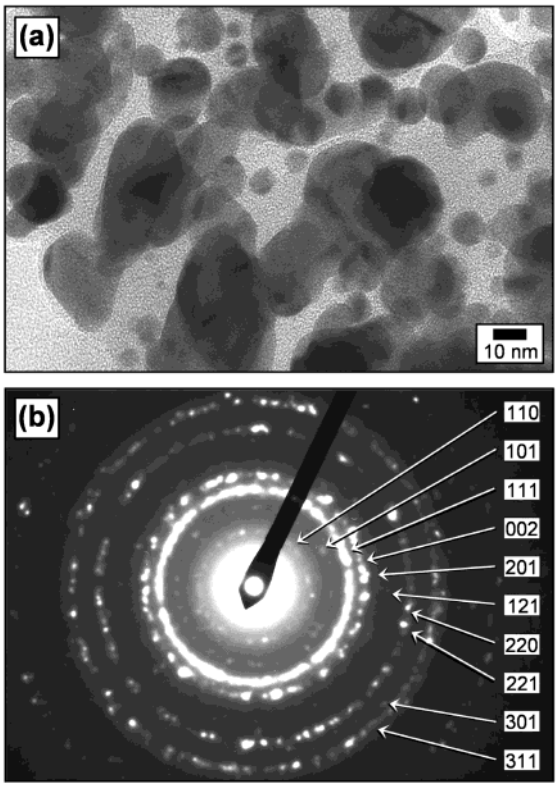

Figure 9. TEM micrograph of atomically ordered $AuCu_3$ nanocrystals is shown in (a), and the corresponding electron diffraction pattern is shown in (b). The electron diffraction pattern highlights the cubic symmetry and superlattice of the ordered $AuCu_3$ structure.

The visible absorption spectra for dilute solutions of atomically ordered AuCu and $AuCu_3$ nanocrystals are shown in Figure 10, along with the corresponding absorption spectra for preannealed AuCu and $AuCu_3$ for comparison. The absorption profile for atomically ordered AuCu looks similar to that of AuCu prior to annealing from 600 to 800 nm, but the sample annealed at 275 °C shows a clear difference in absorption from 400 to 550 nm. For $AuCu_3$, the primary difference in absorption between the preannealed and atomically ordered nanocrystals occurs between 550 and 700 nm.

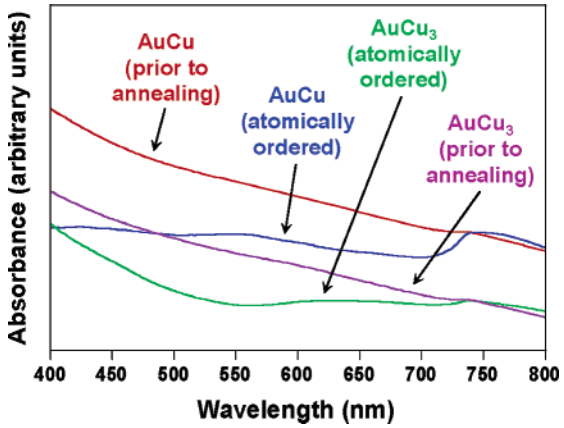

Figure 10. Visible absorption spectra for dilute solutions of AuCu and $AuCu_3$ nanocrystals both before and after annealing. The absorption feature near 735 nm is an instrumental artifact.

Conclusions

In this paper, we have demonstrated a new low-temperature approach to the synthesis of atomically ordered nanocrystals using bimetallic nanoparticle precursors. By utilizing precursors containing zerovalent metals that are modulated on the nanometer scale, solid−solid diffusion is not rate limiting, so low reaction temperatures can be used. Avoiding high-temperature annealing minimizes sintering, and the crystalline nanoparticles can be redispersed in solution for high-volume applications. The stoichiometry of soluble metal salts introduced during nanoparticle synthesis defines the final composition and structures that form upon annealing, which provides easy access to multiple regions of the binary phase diagram. Since diffusion clearly precedes nucleation in the bimetallic precursors that are elementally modulated on the nanometer scale, it is possible to synthesize ordered intermetallic nanocrystals near 200 °C without a high-temperature annealing step. Indeed, this phenomenon of low-temperature nanometer-scale diffusion and nucleation is well understood in planar elemental superstructures of atomic thicknesses[17] and has been used by Johnson and coworkers to synthesize a wide range of new solids at low temperatures[18] and to understand reaction pathways in solid-state systems.[19] Our bimetallic nanoparticle precursors can be viewed as isotropic analogues of Johnson's elementally modulated thin films, and the observed temperature-dependent reactivity is consistent with this comparison. Thus, we expect that our approach to the synthesis of atomically ordered nanocrystals will be applicable to a wide range of inorganic solids, perhaps even yielding new metastable solids that are not stable in bulk systems.

Acknowledgment. We thank Zhiping Luo at the Microscopy and Imaging Center for help with acquiring the TEM images and Francois Gabbai for use of the UV−visible spectrophotometer. This work was supported by start-up funds from Texas A&M University.

JA031547R

(17) (a) Novet, T.; Johnson, D. C. *J. Am. Chem. Soc.* **1991**, *113*, 3398−3403. (b) Noh, M.; Thiel, J.; Johnson, D. C. *Science* **1995**, *270*, 1181−1184.
(18) (a) Schneidmiller, R.; Hornbostel, M. D.; Johnson, D. C. *Inorg. Chem.* **1997**, *36*, 5894−5899. (b) Johnson, C.; Sellinschegg, H.; Johnson, D. C. *Chem. Mater.* **2001**, *13*, 3876−3881. (c) Williams, J. R.; Johnson, D. C. *Inorg. Chem.* **2002**, *41*, 4127−4130.
(19) (a) Noh, M.; Johnson, C. D.; Hornbostel, M. D.; Thiel, J.; Johnson, D. C. *Chem. Mater.* **1996**, *8*, 1625−1635. (b) Oyelaran, O.; Novet, T.; Johnson, C. D.; Johnson, D. C. *J. Am. Chem. Soc.* **1996**, *118*, 2422−2426.